Chapter-3: Study of Structure and Ion Dynamics…..

3.1 Introduction

It has been already discussed in chapter 1, that lanthanum aluminate (LAO) is one of the promising materials for electrolyte for SOFC over other electrolytes like $LaGaO_3$, YSZ and ceria based material. It has a perovskite (ABO_3) structure with octahedron BO_6. Also, it was reported that it has rhombohedral at room temperature and cubic at nearly 500 ºC. It has molecular weight 213.89, melting point 2080 ºC and density 6.52 g/cm^3.

In this chapter, It has been described ion dynamic behaviors of LAO. Since, LAO is an ion conducting material so, in order to understand its ionic conducting behavior, it is necessary to study the ion dynamics. Different groups and workers have tried various approaches to understand ion dynamics in a number of systems, such as glasses, polymers, semiconductors, nano-composites and poly-crystals, etc. and succeed to explore mechanism of conduction. Besides this, to understand the ion dynamics of this material in the measured temperature range, scaling of the conductivity spectra has been done and discussed and confirmed by modules spectra. Also, structural part of LAO has been briefly mentioned on the basis of XRD, SEM and TEM micrograph.

3.2 Experimental

Lanthanum aluminate (LAO) was prepared by auto-combustion synthesis using lanthanum nitrate, $La(NO_3)_3.6H_2O$ (Alfa Aesar), aluminium nitrate, $Al(NO_3)_3.6H_2O$ (Alfa Asear) as cation precursors and citric acid ($C_6H_8O_7.H_2O$) (Merck) as a fuel. All the precursors having purity more than 99% were used. A detailed synthesis and characterization procedure have already been discussed in chapter 2.

Simultaneous differential thermal analysis (DTA) and thermo gravimetric analysis (TGA) of the ash prepared powder was carried out using Netzsch STA 449 F3, Germany

at a heating rate of 10 °C/min up to 1,000 °C in the oxygen atmosphere. Powder X-ray diffraction (XRD) pattern was recorded using Rigaku Miniflex II Desktop X-ray Diffractometer. The density of each composition was measured by Archimedes Principle employing Mettler-Toledo density measurement kit attached to weighing balance. To understand the chemical state XPS spectra of a few compositions was studied. The surface structure was investigated by Field Emission Scanning Electron Microstructure (FESEM, QUANTA 200F). Morphology of the calcined powder was examined by TECHNAI G^2 20G TWIN, Transmission Electron Microscope (TEM). Electrical measurements were performed on the silver coated pellet using two probe methods in the frequency range 20 Hz to 1 MHz using Wayne Kerr 6500P LCR meter in the temperature range 300–750 °C in the air.

3.3 Result and Discussion

3.3.1 Thermal Analysis

In order to estimate the crystallization temperature, Plots of simultaneous DTA and TGA of ash prepared powder, in the temperature range 25–1000 °C was performed which is shown in Fig. 3.1. TGA curve (blue color) shows that the sample loses weight rapidly at 400 °C followed by a gradual decrease in weight up to nearly 700 °C. Also, it shows loss in weight of sample about 25% of its original weight. Corresponding to weight loss in TGA curve, a series of three exothermic peaks are also observed in the DTA curve (red color), one pronounced peak at about 400 °C and two broad peaks at about 470 °C and 600 °C, respectively. These may be attributed to the crystallization, loss of residual citric acid and burning off the carbonaceous materials. No change is found in DTA and TGA curves above 700 °C. This shows the formation of well crystallized LAO at about 700 °C. Based on DTA and TGA results, ash was ground and calcined at 700 °C for 4h.

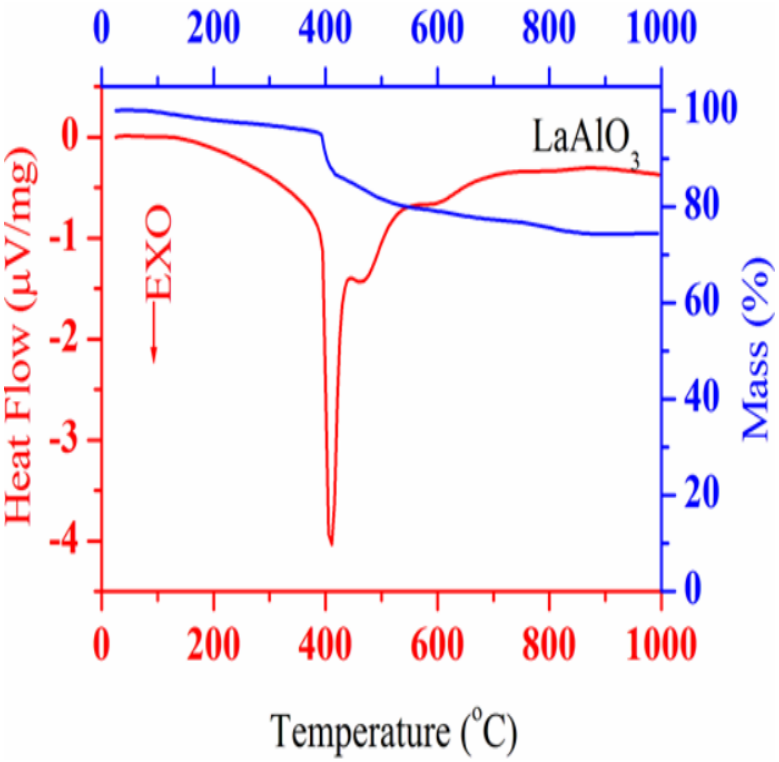

Figure 3.1: Simultaneous DTA and TGA curve of ash prepared LAO

3.3.2 Crystal Structure, Density and Microstructure

To observe the phase purity and crystal structure of the calcined and sintered samples, powder XRD measurement was performed and shown in Fig. 3.2(a) and Fig. 3.2(b), respectively. XRD patterns clearly reflect the single phase formation of LAO and well matches with JCPDS file no 82-0478. The similar structure was also reported by Derighettiet al.. Lattice parameters were obtained using a full pattern Lebail refinement of powder X-ray diffraction pattern of sintered powder of LAO with rhombohedral structure in the R-3c space group and found to be a = b = 5.3545(19); c = 13.1276(93), $\alpha = \beta = 90$; $\gamma = 120$. Again, Rietveld refinement of the system was done and shown in the Fig. 3.2(c). The only difference in the XRD pattern of the calcined and sintered samples is the sharpness of their peaks. The broader peaks in the x-ray pattern of the calcined sample show smaller crystallite size, whereas the sharper peaks in the x-ray pattern of the sintered sample show bigger crystallite size. The bigger crystallite of the sintered sample

is a consequence of collapse of smaller crystallites of calcined powder during sintering to obtain dense and compact pellets for further characterizations.

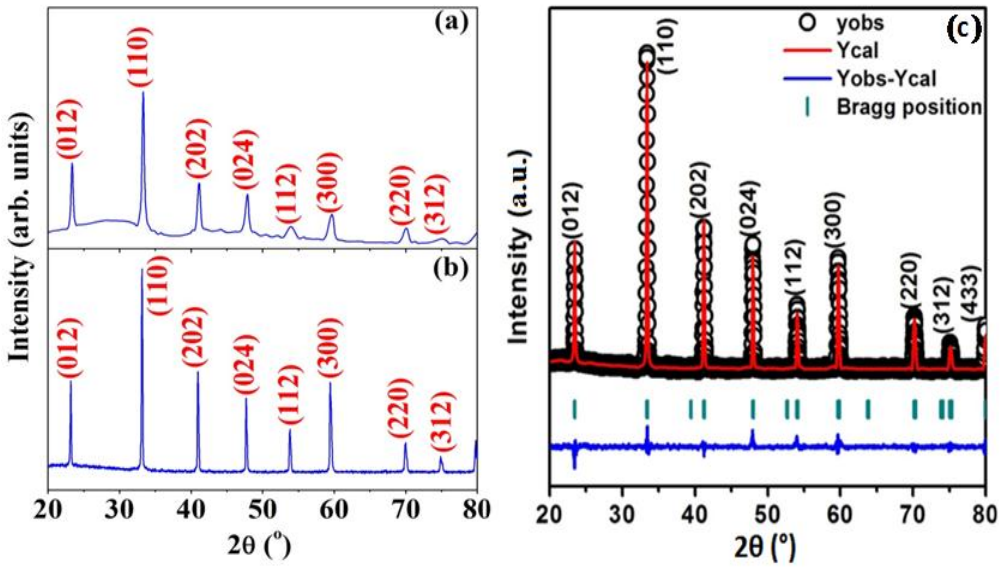

Figure 3.2: Powder X-ray diffraction pattern of **(a)** Calcined **(b)** Sintered powder of LAO and **(c)** Rietveld refinement of LAO

The crystallite size of the LAO was determined using Scherrer' formula

$$t = \frac{0.9\lambda}{\beta \cos\theta}, \qquad 3.1$$

where, t is the particle size, λ is the wave length of CuKα X-ray and β is the full width at half maxima (FWHM). The crystallite size of the ash and calcined powder at 500 °C was found to be about ~48 nm, which increase to ~600 nm on sintering. The measured density of the sintered pellet using the Archimedes Principle has been found to be 95 % of its theoretical value.

3.3.3 Microstructural Study

SEM image of thermally etched pellet sintered at 1300 °C is shown in Fig. 3.3. The micrograph shows that the average grain size is about 2.5 μm with dense structure. The large grain size observed in SEM is due to grain growth during the sintering process.

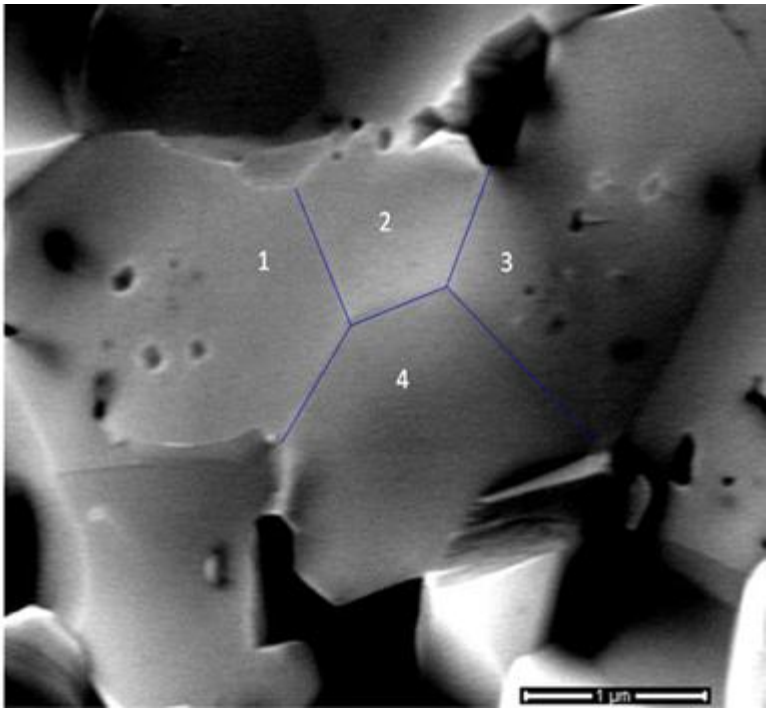

Figure 3.3: SEM micrograph of sintered pellet of LAO

The TEM images, in Fig. 3.4 (a-d), clearly depict that the particles are nearly irregular in shape. The nanocrystals appear mostly as hexagons in Fig. 3.4 (a). On the other hand, it can be clearly seen that the particles are agglomerated to each other in Fig. 3.4 (b). The average diameter of the particles is estimated to be ~74 nm by considering them spherical. The HRTEM image of LAO nanocrystals depicts well defined lattice fringes with an interplanar spacing of 0.27 nm, which corresponds to the (110) lattice plane spacing of LAO nanocrystals as shown in Fig. 3.4 (c). Furthermore, SAED pattern has been displayed in Fig. 3.4 (d) which shows that the LAO nanocrystals have broad diffuse diffraction ring with bright overlapped spotty pattern indicating that the prepared nanocrystals are good polycrystalline in nature. Different spots associated with each specific rings of (hkl) set of reflections (110), (202), (300) and (220) indicate that the lanthanum aluminate nanocrystals have rhombohedral structure as evident from X-ray diffraction peaks.

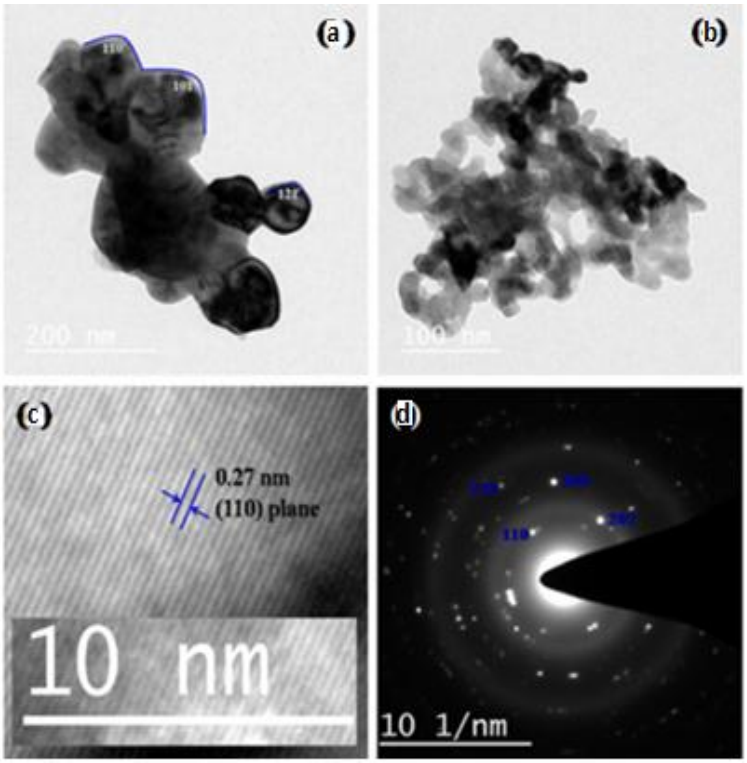

Figure 3.4: (a)-(d) TEM image of calcined $LaAlO_3$ sample

3.3.4 X-ray Photoelectron Spectroscopy

The XPS spectra (Fig. 3.5) of La 3d, Al 2p and O 1s were analyzed for the investigated system LAO. All signal peaks were calibrated with C 1s at around 284.6 eV. The core and satellite peaks of La $3d_{5/2}$ and La $3d_{3/2}$ were observed with the binding energy of ~834.9 eV and ~851.6 eV respectively, which is in good agreement with other reported value in literature [12]. The peak $3d_{5/2}$ corresponds to the state La^{3+} in the system. The additional peak in the state $3d_{3/2}$ at high energy is attributed to the oxidized lanthanum species. The peak of the binding energy corresponding to the Al^{3+} in the Al 2p spectra was at 72.5 eV. Oxygen reacts with Al rather than La, due to the low binding energy of Al. A sharper peak of oxygen (O 1s) has been observed with high binding energy ~532 eV attributed to the incorporation of oxygen into LAO system and its reaction with Al and La atoms that occupy the oxygen vacancy sites changing the bond structure of LAO system. This is the characteristic state peak of the O^{2-} ions. Thus, the

XPS spectra of LAO confirm that the constituents are present in their characteristic chemical state in the system.

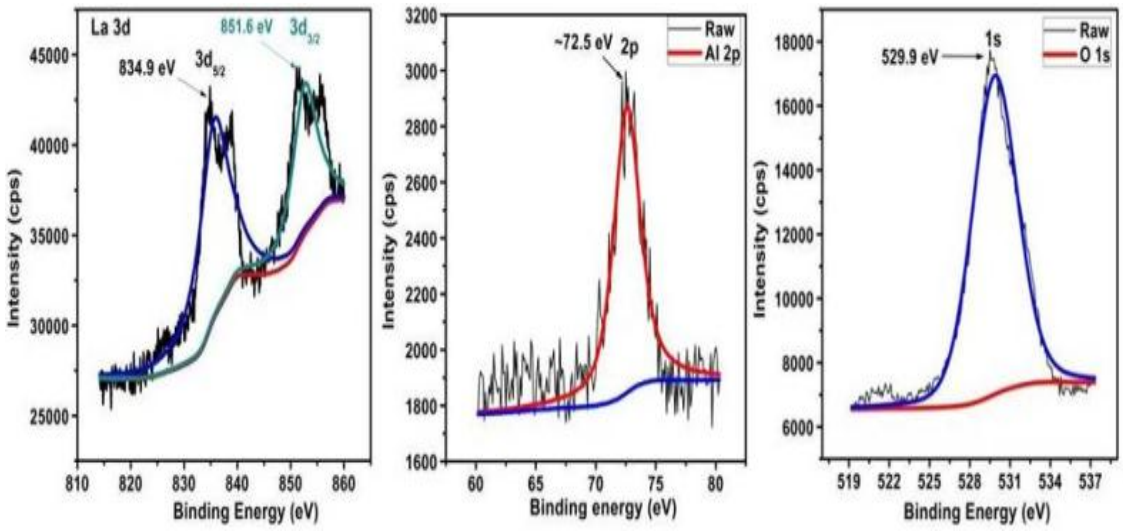

Figure 3.5: XPS of Lanthanum Aluminate

3.3.5 Electrical Property

The frequency dependent conductivity spectra of LAO at various temperatures are shown in Fig. 3.6. The symbols in this figure represent the experimental data and the solid lines represent fit to the data points by equation (2.1). The above figure clearly shows the first plateau corresponding to bulk conductivity (σ_{dc}) caused by the random motion of the mobile charge carriers, and the dispersion regime assigned to the ac conductivity caused by the correlated forward-backward hopping motion of the charge carriers. In the present case, the second plateau in the high frequency regime, as mentioned earlier, could not be observed due to the limited frequency range available and window effect, also. The conductivity (σ_{dc}) and the exponent factor (n) were obtained by fitting of data points to the equation (2.1) at all the measured temperatures.

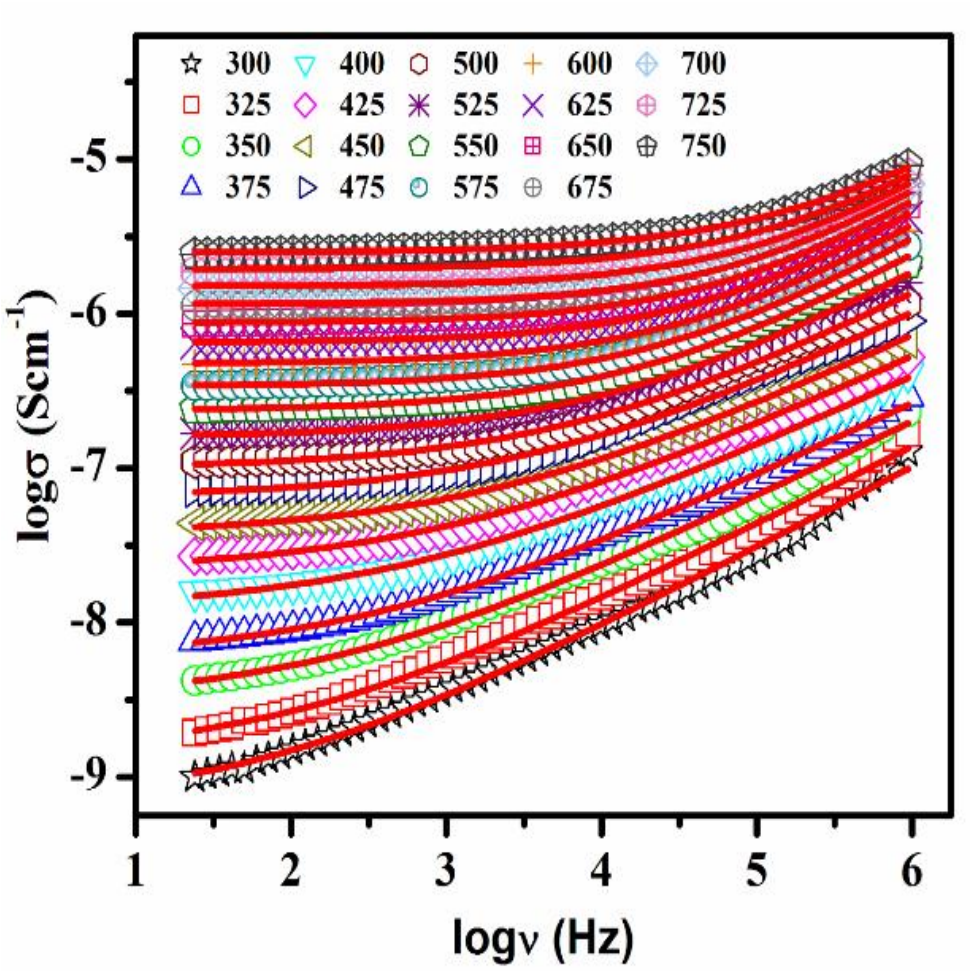

Figure 3.6: Conductivity spectra of LAO at a few temperatures (ºC). Symbols denote the experimental data points and the solid lines represent the fit to the data points with equation

The reciprocal of temperature dependence of bulk conductivity (σ_{dc}) and hoping frequency (ν_H) are shown in Fig. 3.7 (a) and Fig. 3.7 (b). These plots show the Arrhenius behavior. The activation energy (E_H = 0.92 eV) for hopping obtained by a least square linear fit of data points of Fig. 3.7 (a) is close to the activation energy (E_σ = 0.99 eV) of the bulk conductivity (σ_{dc}) found from the least square linear fit of the data points of Fig. 3.7 (b). This indicates that the concentration of the mobile charge carriers is independent of temperature and hence, the conductivity is determined primarily by the mobility of the charge carriers [77]. The value of the activation energy for bulk conductivity implies conduction is due to oxide ion through oxygen vacancies [78].

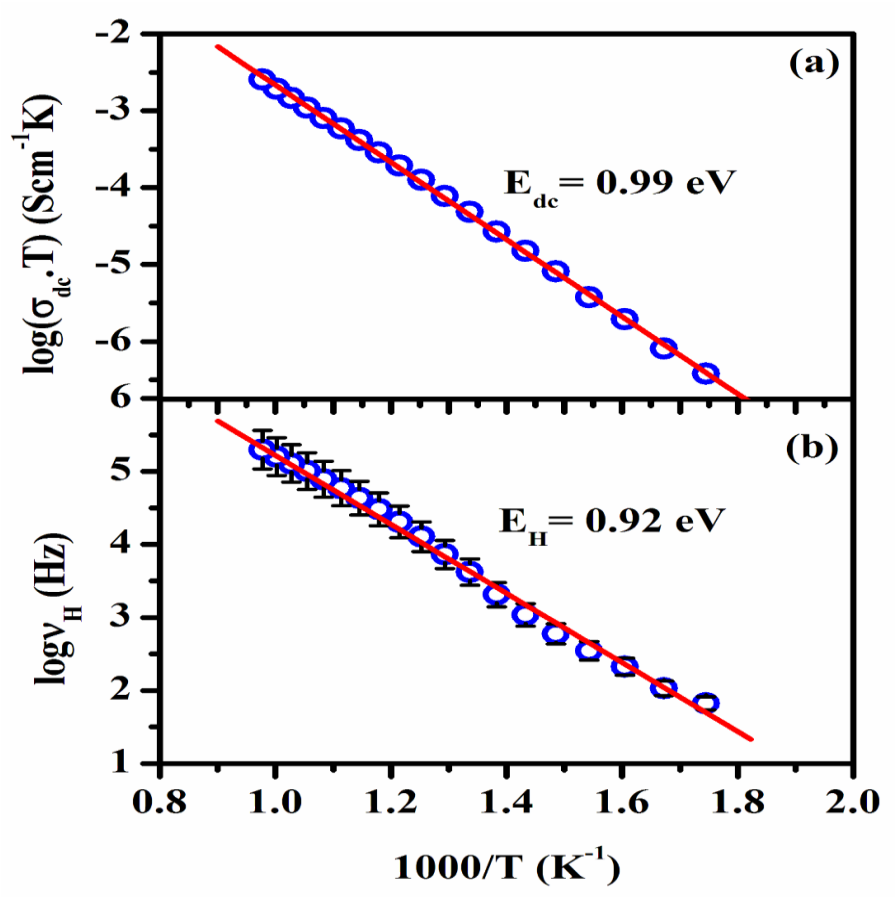

Figure 3.7: Arrhenius representation of **(a)** dc conductivity and **(b)** the hopping frequency for LAO

Moreover, to examine the correlation between bulk conductivity (σ_{dc}) and hoping frequency (ν_H) the logarithmic plot was drawn between these two parameters as shown in Fig. 3.8. The above figure clearly shows the linear dependence of these parameters on each other with a slope of almost unity. This implies that the dc and ac conductions are correlated in LAO. This type of behavior is also reported by Ahmad et al. in polycrystalline $PbSnF_4$ and by Ghosh et al. in lithium telluride glasses.

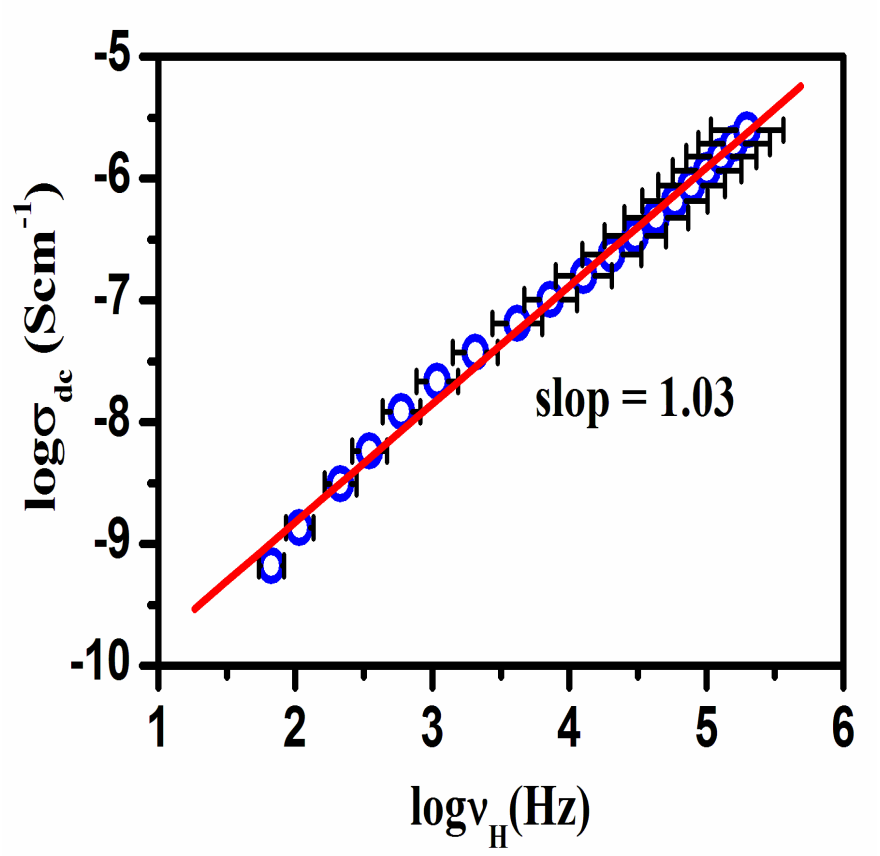

Figure 3.8: The dc conductivity, σ_{dc} vs. hopping frequency, ν_H for LAO

To gain insight into temperature dependence of conduction mechanism, the scaling behavior of frequency dependent conductivity has been studied. For the present investigation Ghosh scaling has been applied in which hopping frequency has been taken as a scaling factor. The scaled spectra of LAO at different temperatures are shown in Fig. 3.9. It can be seen that all the spectra at different temperature merge onto a single master curve with negligible deviation. The negligible deviation may have been observed due to window effect as a consequence of limited available frequency range. The merger of different curve onto a single master curve indicates that LAO obey the time temperature superposition principle in the entire temperature and frequency ranges. Thus, the dynamic of oxide ions in LAO is independent of temperature. Also, the superposition of different spectra to a master curve for LAO may be result of unchanged dimensionality of the conduction pathways.

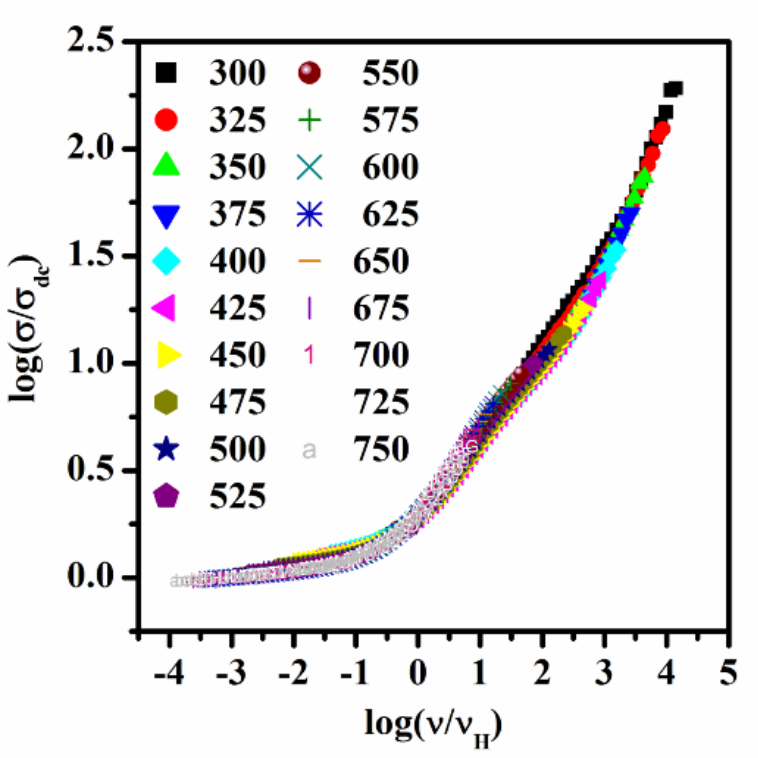

Figure 3.9: Scaled conductivity spectra of LAO at various temperatures (°C)

It has been mentioned in introduction that some groups prefer the interpretation of ion dynamics with the help of modulus spectra. This method was introduced by Macedoet al. to explore the ion dynamics in ion conducting materials by eliminating the electrode polarization effect. Fig. 3.10 shows the imaginary part of the modulus spectra for LAO at few temperatures. This spectrum shows a single relaxation peak which is asymmetric in nature. It is also seen that M" spectra is much border than the Debye peak, which can be attributed to the distributed relaxation times. The conductivity relaxation frequency, ν_{max}, corresponding to M''_{max}, gives the most probable relaxation time, τ_{max}, and can be obtained by the relation $\nu_{max}\tau_{max}=1$ which holds at the peak of the relaxation curve. The region to the left of this peak represents the region in which the long range motion of ions takes place while the region to the right of this peak corresponds to the localized forward-backward hopping of the ions. With the increasing temperature, movement of the charge carriers becomes faster and consequently they possess decreased relaxation time and

hence shift of the peak value towards higher frequencies observed. Thus, it can be concluded that the relaxation process is thermally activated and charge carrier hopping is taking place in LAO.

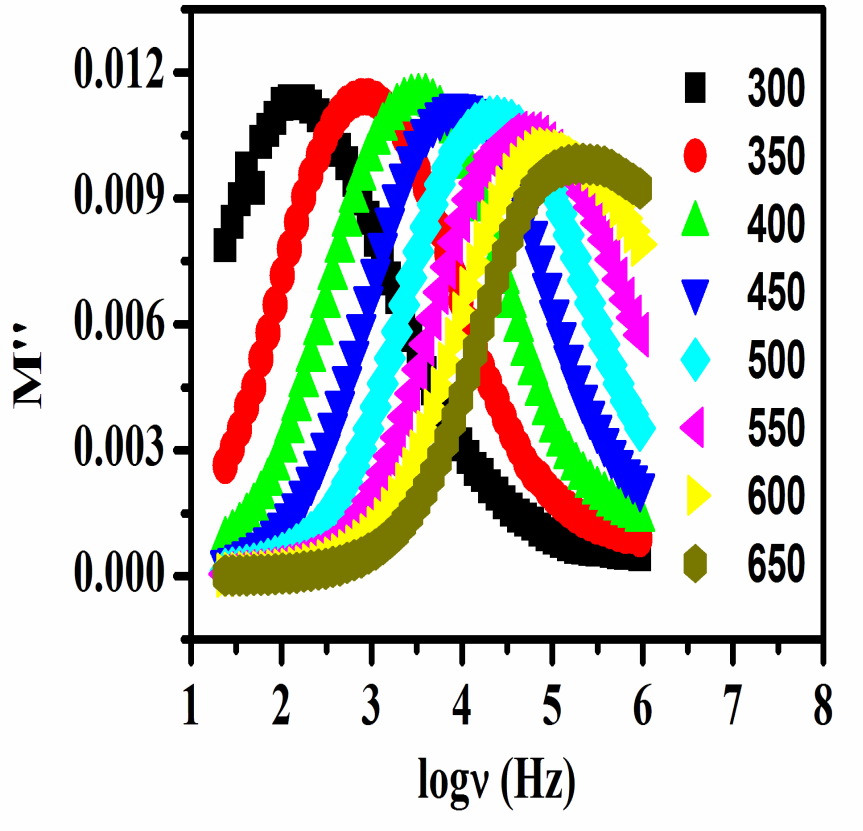

Figure 3.10: Electric modulus spectra of LAO at various temperatures (°C)

For the better understanding of relaxation dynamics, here scaling behaviour of the modulus spectra have also been utilized. Fig. 3.11 shows scaled spectra of LAO in which axis of the imaginary modulus has been scaled by M''_{max} and axis of the frequency has been scaled by ν_{max}. From the figure it can be seen that the spectra at different temperature are nearly overlapped onto a single master curve. This indicates that the dynamical process controlling the conductivity relaxation is same over the entire temperature range of measurement.

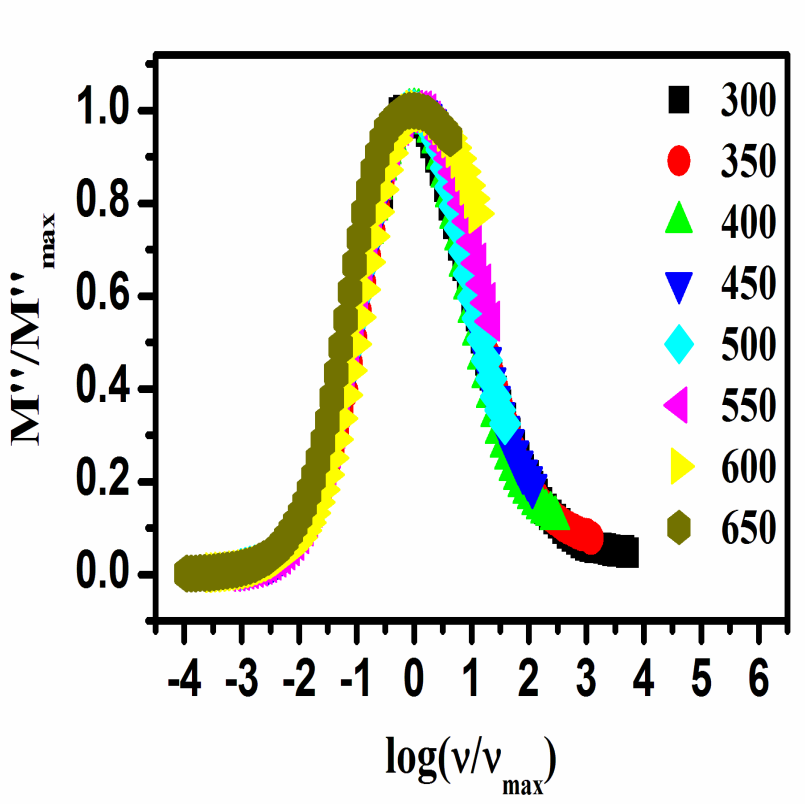

Figure 3.11: Scaled electric modulus spectra of LAO at various temperatures (°C)

Fig. 3.12 represents the Arrhenius plot of ν_{max} for LAO. The symbol shows the data points corresponding to peak frequency obtain from the Fig. 3.10 and the solid line shows the linear fit to the data points. The activation energy, $E_{\nu max}$ calculated from the slope was found to be 0.90 eV. When comparing it with the values of the activation energy shown in Fig. 3.7 (a) and Fig. 3.7 (b) for dc conductivity and hopping frequency then one can see that these values are closer to each other. The closer value of activation energy of E_H and $E_{\nu max}$ indicate that the hoping frequency, ν_H, and the peak frequency, ν_{max}, provide the limit at which short range hoping motion is changing into the long range percolation.

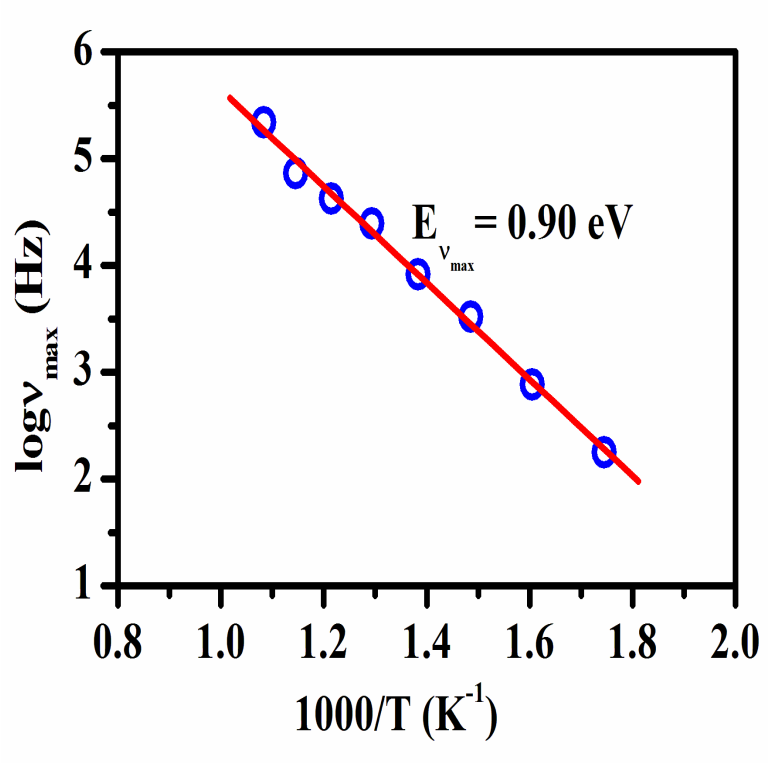

Figure 3.12: Arrhenius representation of peak frequency of electric modulus spectra for LAO

Thus, from the above discussion, it can be concluded that the scaling behavior of the modulus spectra supplements the findings obtained by the scaling behavior of the conductivity spectra. Here, we found that in Fig. 3.7 (a) and Fig. 3.7 (b) there was a dual slope nature. This indicates that there may be a transition nearly 500 ºC which compel me for further study in the next chapter.

3. 4 Conclusions

Lanthanum aluminate has been prepared successfully by citrate nitrate auto combustion route. The Thermal analysis and powder X-ray diffraction pattern showed the single phase formation of LAO at 700 °C with rhombohedral perovskite structure with space group R-3c. SEM observation clearly shows that the grains have distorted rhombohedral shape which is also justified by TEM. The crystallite size and grain/particle size is found to be ~47 nm and ~74 µm, respectively. HRTEM analysis exhibits the interatomic spacing is 0.27 nm corresponds to (110) plane of a rhombohedral lattice of

LAO nanocrystals. SAED analysis also confirms the well polycrystalline rhmbohedral structure of LAO nanocrystals. The XPS spectra of LAO confirm that the constituents are present in their characteristic chemical state in the system.In this system, the charge carriers are temperature independent and the conductivity is mainly depending on the mobility of the charge carriers. Oxide ions are mainly involved in the conduction as the charge carrier. The dc and ac conductions are correlated in LAO. The scaling of the conductivity spectra follows the Gosh scaling. This indicates that the hopping frequency is a suitable scaling parameter for LAO. The Scaling property is also observed in the modulus spectra of LAO.